

Development of a novel phase-field method for local stress-based shape and topology optimization



Seung Hyun Jeong^a, Gil Ho Yoon^{b,*}, Akihiro Takezawa^c, Dong-Hoon Choi^b

^a Graduate School of Mechanical Engineering, Hanyang University, Seoul, Republic of Korea

^b School of Mechanical Engineering, Hanyang University, Seoul, Republic of Korea

^c Division of Mechanical System and Applied Mechanics, Faculty of Engineering, Hiroshima University, Japan

ARTICLE INFO

Article history:

Received 10 March 2013

Accepted 8 November 2013

Available online 8 December 2013

Keywords:

Stress-based topology optimization

Phase-field method

Augmented Lagrange multiplier method

Topological derivative

ABSTRACT

This research develops a stress-based topology optimization method (STOM) using the phase-field method representing topological changes. This research shows that to apply the phase field method, regional and localized stress constraints should be addressed. Thus, we use an Augmented Lagrange multiplier approach for the stress constraints and present a new numerical solution for the Lagrange multipliers inside the Allen–Cahn equation with the topological derivatives. Through several two dimensional illustrative problems, the results of the phase-field method have larger objective values, but are robust from a stress point of view compared with the results of the STOM by the density method.

© 2013 Elsevier Ltd. All rights reserved.

1. Introduction

Limiting the maximum nominal stress of linear and nonlinear structures has become an important engineering problem [1–10]. When nominal stress (either due to a static or dynamic load) exceeds a certain limit, static fracture or dynamic fatigue failure leading to catastrophic disasters occurs. To prevent these failures, a practical engineering approach is to calculate the nominal stress values of a structure of interest by finite element method and to confine them to a certain maximum value by changing the geometry or the material of a structure of interest. Furthermore, size and shape optimizations for stress constraints have been researched for a long time, and these results are commonly applied to obtain safer and more robust designs from mathematical and engineering points of view. The use of topology optimization (TO) methods to consider local stress constraints defined at every finite element is a recent achievement. This research contributes to these optimization researches by presenting a new stress-based shape and stress-based topology optimization method (STOM) using the phase-field method that expresses topological changes in a design domain with explicit phase-field curves. Despite some relevant works on STOM with the density design variables or the level set function variables [1–4,6–13], optimization methods minimizing volume subject to stress constraints defined at all finite elements (hereafter local stress constraints) have not yet been proposed using the phase-field method due to several difficulties.

1.1. Issues for local stress constraints

In conducting the stress-based topology optimization, the three well-known difficulties, i.e., the singularity problem, the local constraint problem, and the highly nonlinear behavior of stress constraints, should be properly addressed [1–4,6–10,14–17]. The singularity behaviors of the stress constraints in TO have been addressed [4,6,14,15,17]. According to the previous researches, stress singularities arise when some design variables of the SIMP method converge to the lower bound (i.e., 0.001 or 0.0001) to simulate non-structural regions (“void” regions). To resolve this issue, there have been many proposed solutions and relaxation methods such as the *epsilon* relaxation method [4,17], the *qp*-relaxation method [1,2], and the relaxed stress indicator method [6]. Second, as the nominal stress values of all finite elements of interest must be constrained, from a computational point of view there are too many constraints to efficiently solve the optimization problem with a dual optimizer. As the computational cost for the sensitivity analysis and the sub-optimization increases, one must resort to approximation methods and other remedies. One of the methods is the constraint selection method, which selects only active stress constraints and calculates their sensitivity values [4]. Recently, the global stress measure methods have been proposed [6,9,18]. Until now, the popular two proposals are the *p*-norm approach and the Kreisselmeier–Steinhauser (KS) approach. In this paper, the *p*-norm approach is employed with a correction or scaling factor (see [6,8,9,18] for more detail). In addition, with only one global constraint measure, it is impossible to consider the effects of the localized stress constraints accurately. Thus a method of dividing the design domain into several sub-

* Corresponding author. Tel.: +82 22200451.

E-mail addresses: ghy@hanyang.ac.kr, gilho.yoon@gmail.com (G.H. Yoon).

regions and calculating the global stress measures at each domain is employed in this research [6,8,9]. For the third issue, it is important to appropriately consider the highly nonlinear behavior of the stress constraints due to the relaxation, the penalization of the design variables of TO [19], and the global stress measure. To resolve this issue, an efficient and accurate dual sequential approximate optimization (SAO) method should be employed. We will discuss each of these issues as they relate to our phase-field method approach.

1.2. Post-processing issues

The post-processing problem is also important in the stress-based topology optimization problem. From a mathematical point of view, the original TO problem of finding the so called “solid” and “void” domains inside a design domain is a binary optimization problem that is almost impossible to apply to practical engineering problems. Therefore, it has been common to *relax* the problem by introducing the continuous design variables of the homogenization method or using the Solid Isotropic Material with Penalization (SIMP) method. With such a relaxation, it becomes possible to obtain optimal topological layouts within a reasonable computation time, but a post-processing of the final layouts with the intermediate design variables of the relaxed TO problem should be completed. Fig. 1 shows a crude post-processing result of an L-shaped beam structure using the SIMP method and the hard-kill post-processing which sets the design variables to 1 or 0 depending on a threshold value, which is 0.5 in Fig. 1. As shown in Fig. 1(b), the maximum stress value may be severely increased after the postprocessing. Therefore, to represent layouts more precisely and explicitly during and after TO, some applications of the level set method [20–22] or the phase-field method [23] have been proposed. As some explicit curves between the solid and void domains are parameterized and optimized, the intermediate design variables are less presented, and the post-processing becomes relatively straightforward. Thus, this research addresses intermediate design variables and post-processing with the phase-field method, and investigates the differences between the density-based method and the phase-field method from a structural point of view.

1.3. Augmented Lagrange multipliers for multiple stress constraints

To the best of our knowledge, the previous works with the phase field method has considered the case of only one constraint, such as a volume constraint. Usually, a structural performance measure such as compliance, target displacement or the weighted sum of squares of the eigenfrequencies is chosen [22–24]. However, the stress-based TO with the p -norm stress measures in multiple sub-regions, the mathematical consideration of multiple constraints becomes an important issue [6,9,11,18]. To resolve this issue in the phase field method, this research presents an Augmented Lagrange multiplier (ALM) method to transform an optimi-

zation problem with multiple constraints into an optimization problem with a single objective function without constraints by employing Lagrange multipliers.

1.4. Design space comparison

As another issue, the differences in the size of the design spaces between the phase-field method and the SIMP method should be considered. Compared with the design space of the SIMP method, the design space of the phase-field method is smaller. To enlarge the limited design space of the phase-field method, heuristic topological derivative methods have been developed [25,26]. Although the mathematical formulations of the topological derivative methods are highly sophisticated, their implementation with finite element methods becomes heuristic. Furthermore, it is likely that despite the introduction of topological derivative methods, it is still difficult to obtain better designs than the SIMP method. Thus, it is natural for us to study the differences in the design spaces of the SIMP method and the phase-field method. Our concern regards the effect of the smaller design space of the phase-field method on the optimal layout in the stress based topology optimization. In particular, we investigated the following two questions. Firstly, the differences of highly stressed regions in the phase-field method and the SIMP approach are investigated. From the previous discussions [6,11], it seems that smooth curves and features can be obtained in the SIMP method to prevent stress concentration, and the question is whether the same is true of the phase-field method. Secondly, we analyze the roles of the internal members of the optimized layouts. In other words, we want to investigate whether internal members appear to minimize compliance or confine stress values. Furthermore, we also derived and implemented a new formulation for the regional stress constraints of the topological derivative method. The phase-field method with an explicit curve function has a smaller design space compared with SIMP-based topology optimization. For this reason, as iterations proceed, there is a tendency in the phase-field method to erase void regions, which in turn limits the design space. To resolve this issue, we propose a topological derivative method that heuristically introduces some holes. We calculated and implemented the topological derivatives of the p -norm stress constraint functions per every fixed number of evolution cycles. The detailed procedure will be presented in Section 3.

The remainder of the paper is organized as follows. In Section 2, we give a brief introduction to the phase-field method and its application to general TO problems. Section 3 gives the formulation of the stress-based TO problem we consider and a detailed description of the proposed optimization procedure using the ALM and topological derivatives via the phase-field method. The usefulness of the present method will be verified by solving several structural optimization problems in Section 4. Section 4 also compares the phase-field method with the SIMP method. Finally, the conclusion summarizes our findings.

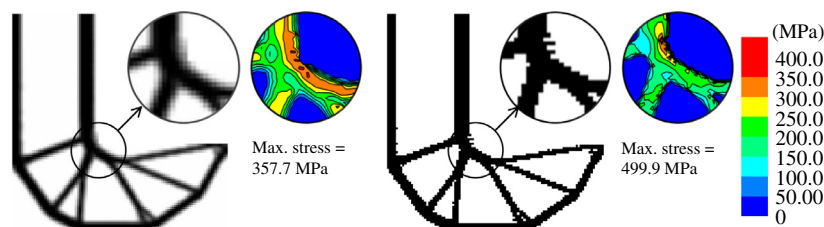


Fig. 1. Crude post-processing of the intermediate design variables from a stress point of view.

2. The application of the phase-field method for topology optimization

In this section, a brief explanation of the phase-field method and its application to a typical TO problem are discussed and some details on minimizing compliance subject to a volume constraint are in the Appendix. A detailed explanation of the phase-field method can be found elsewhere [23,24,27–33].

2.1. The phase-field function and its evolution equation

A phase-field function $\phi(\mathbf{x})$ is defined over an entire analysis domain and represents the phase of the local points therein, as shown in Fig. 2. From a physical point of view, the phase-field function can be interpreted as the average phase of the local points. To understand the concept of the phase-field method, let us consider a closed system composed of two phases in Fig. 2, one of which

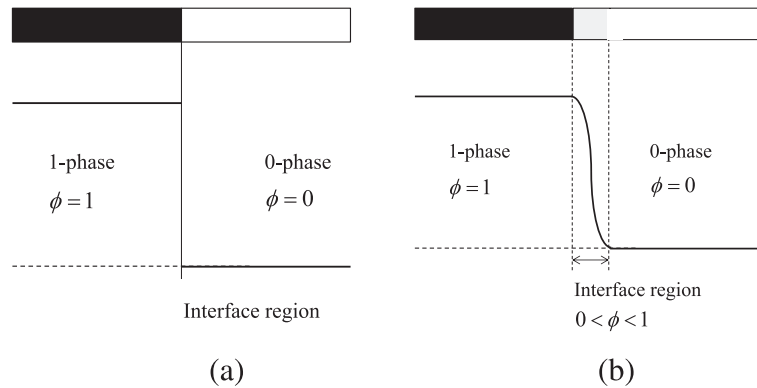


Fig. 2. A solid-void domain representation using the phase-field method. (a) A phase to be represented and (b) a real phase implemented by the phase-field method.

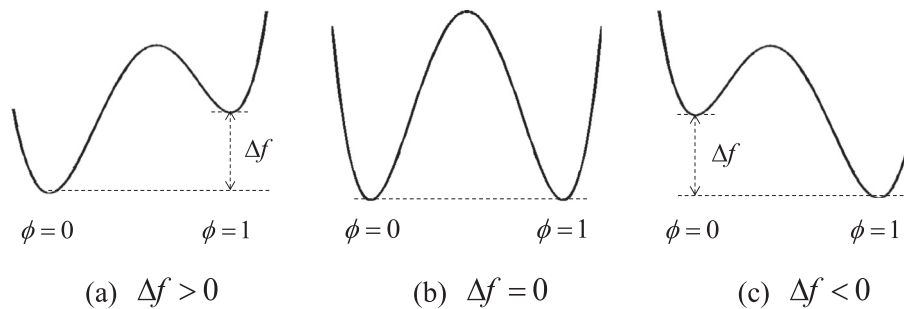


Fig. 3. A graphical description of the double well potential.

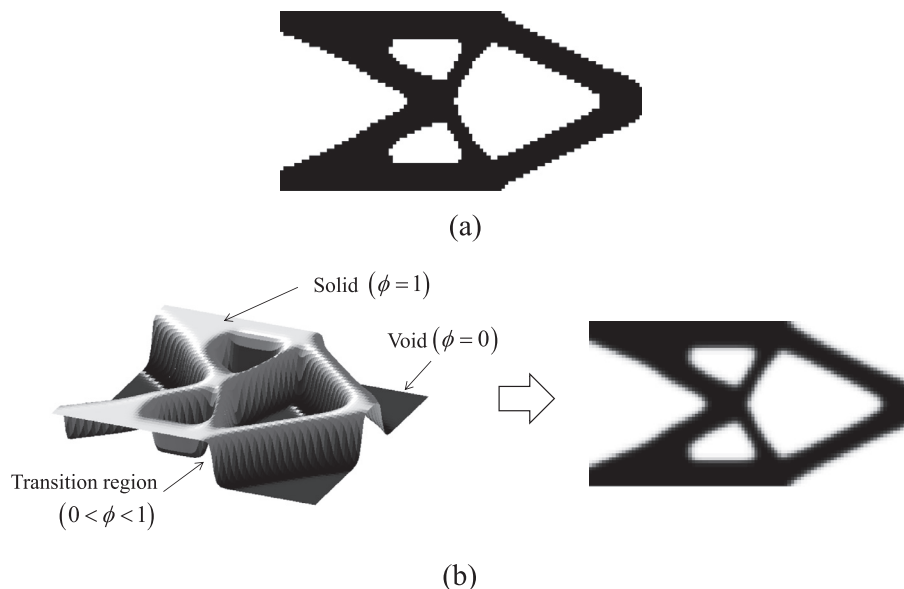


Fig. 4. An illustrative example of topology expression using the framework of the phase-field method: (a) A topology to be referenced and (b) the topology expression of (a) by the phase-field method.

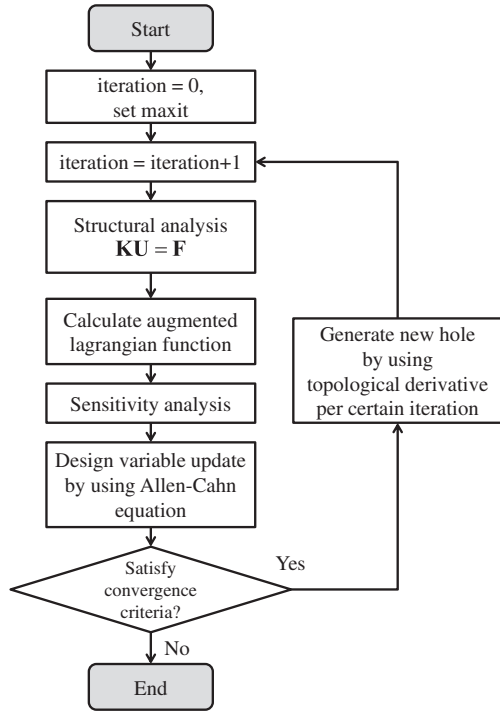


Fig. 5. The present STOM using the phase-field method.

corresponds to a phase of 1, while the other corresponds to a phase of 0. The boundary of each phase is represented as a smooth function that interpolates the different values $\phi(\mathbf{x})$, and is labeled the “diffuse interface”.

The state of a domain may be determined by minimizing the Van der Waals free energy equation as follows:

$$F(\phi) = \int_{\Omega} \left(\frac{\varepsilon}{2} |\nabla \phi|^2 + \varepsilon^{-1} f(\phi) \right) d\mathbf{x} \quad (1)$$

where ε is a small positive parameter scaling the effect of the first and the second terms in (1). The first term in (1) only affects the transition region because its value is zero in the regions of each limit state. The function $f(\phi)$ in the second term is a so-called double-well potential function and is defined as follows [27].

$$f(\phi) = \frac{a^2}{2} g(\phi) + \Delta f \cdot h(\phi) \quad (2)$$

$$g(\phi) = \phi^2 (1 - \phi)^2 \quad (3)$$

$$h(\phi) = \phi^3 (10 - 15\phi + 6\phi^2) \quad (4)$$

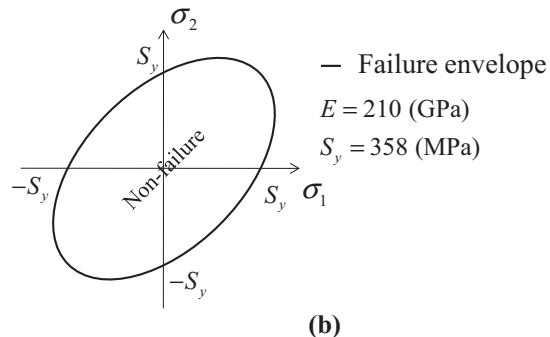
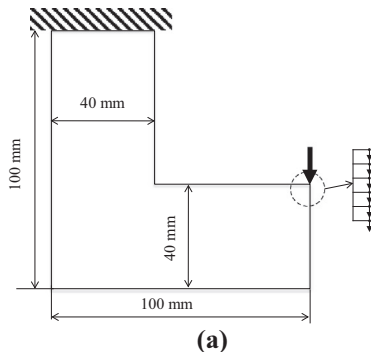


Fig. 6. The L-shape design problem. (a) The design domain, the boundary condition, the loading condition (the load is distributed at the 6 nodes), and (b) the envelope of the von Mises stress of the carbon steel of interest.

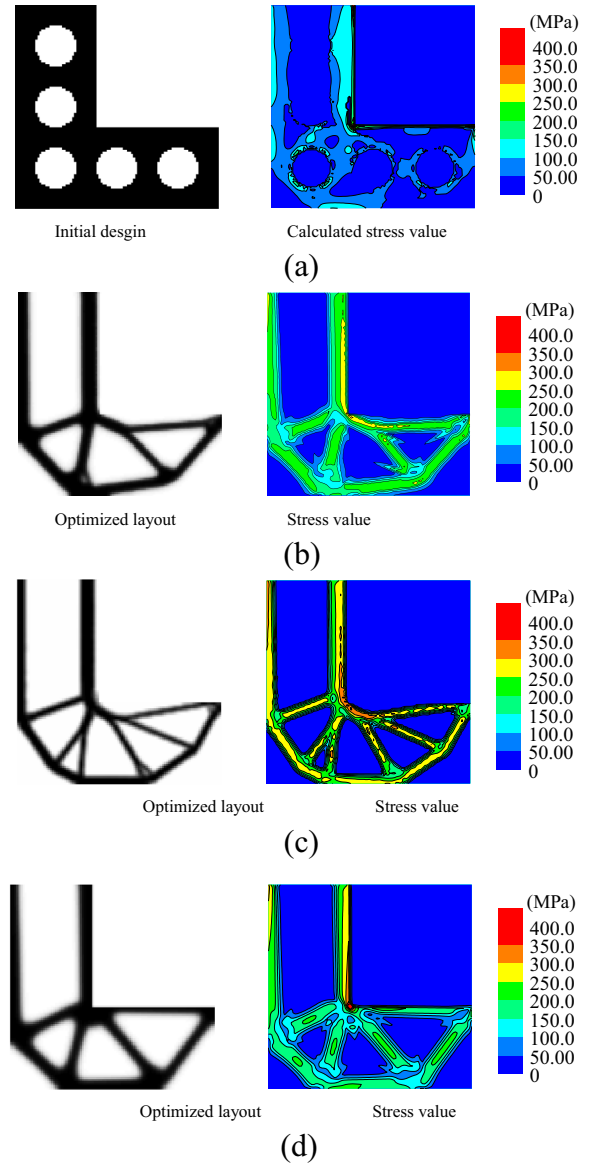


Fig. 7. The optimized layouts of the L-shaped beam: (a) An initial layout and its stress distribution ($\sigma_{\max} = 380.0$ MPa) for the phase-field method, (b) an optimized layout and its stress distribution obtained by the present stress-based topology optimization method using the phase-field method ($V/V_0 = 0.360$, $\sigma_{\max} = 357.9$ MPa), (c) an optimized layout and its stress distribution by the STOM method with a SIMP approach ($V/V_0 = 0.293$, $\sigma_{\max} = 357.7$ MPa), and (d) an optimized layout by minimizing compliance and its stress distribution ($V/V_0 = 0.360$, $\sigma_{\max} = 658.9$ MPa) using a phase-field approach.

As shown in Fig. 3, the double well potential function has local optima when $\phi = 0$ and $\phi = 1$. This means that if Δf is larger than zero, a phase of 0 is more stable than a phase of 1, as shown in Fig. 3(a). In contrast, if Δf is smaller than zero, a phase of 1 is more stable than a phase of 0, as shown in Fig. 3(b). According to Eq. (1), the total free energy can be determined, and the interface layer tends to move to minimize the total free energy. If the value of the double well potential is dominant in the analysis domain with a positive value for Δf , the interface layer tends to move to a phase of 1 because the free energy becomes smaller with a phase of 0 (and vice versa).

To minimize the Van der Waals free energy, the interface region evolves with respect to time as follows:

$$\frac{\partial \phi}{\partial t} = -M(\phi) \frac{\delta F(\phi)}{\delta \phi} \quad (5)$$

where $M(\phi)$ is a variation rate. By substituting Eq. (1) into Eq. (5) and using the definition of a functional derivative, the time evolution equation can be given as follows

$$\frac{\partial \phi}{\partial t} = \varepsilon^2 \nabla^2 \phi - f'(\phi) \quad (6)$$

Eq. (6) is known as the Allen–Cahn equation [34].

2.2. Application of the phase-field method to topology optimization

To simulate topology modification inside a design domain without an alternation of a finite element mesh, the material properties (i.e., Young's modulus for linear static elasticity) are subject to change by the phase-field method. For an illustrative example, let us consider the structure of Fig. 4(a). Rather than removing the finite elements for the non-structural domain expressed by $\phi = 0$, their Young's moduli are set to a very low value limit compared with the Young's moduli of the solid part expressed by $\phi = 1$. Transition regions with a finite thickness between the solid and the void are represented by intermediate values of the explicit curves, i.e., $0 < \phi < 1$.

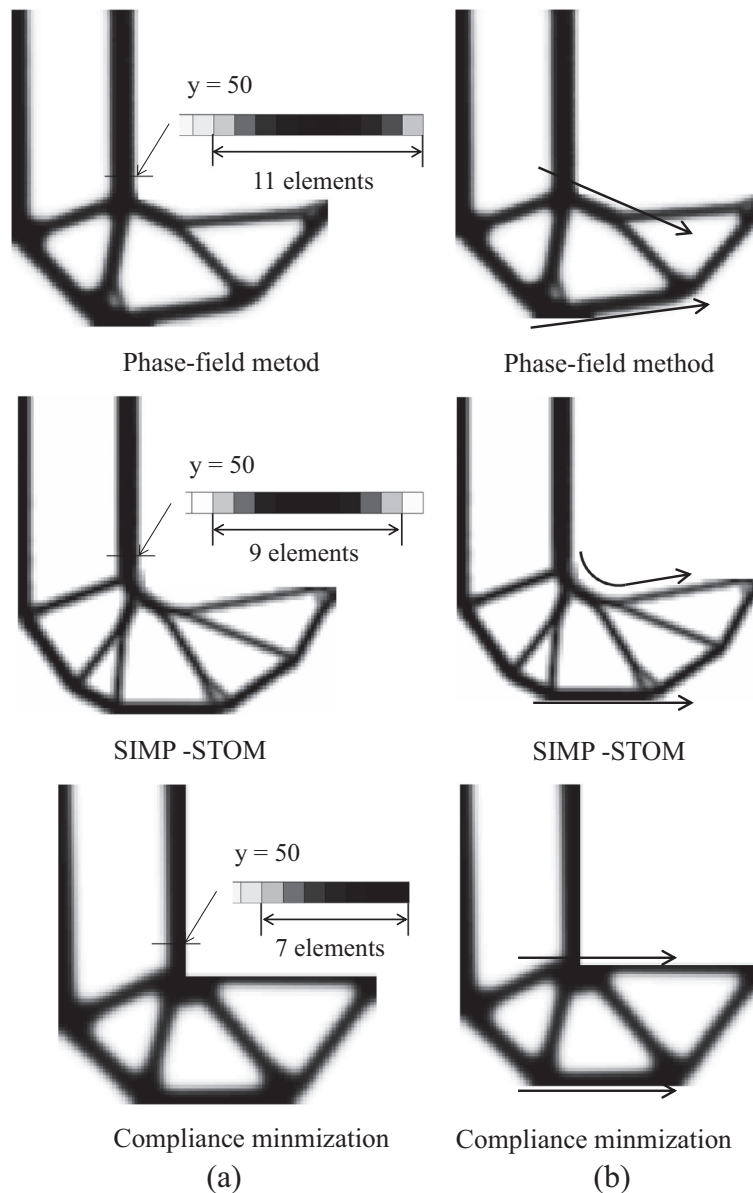


Fig. 8. Some conceptual explanations of the stress distributions of the designs.

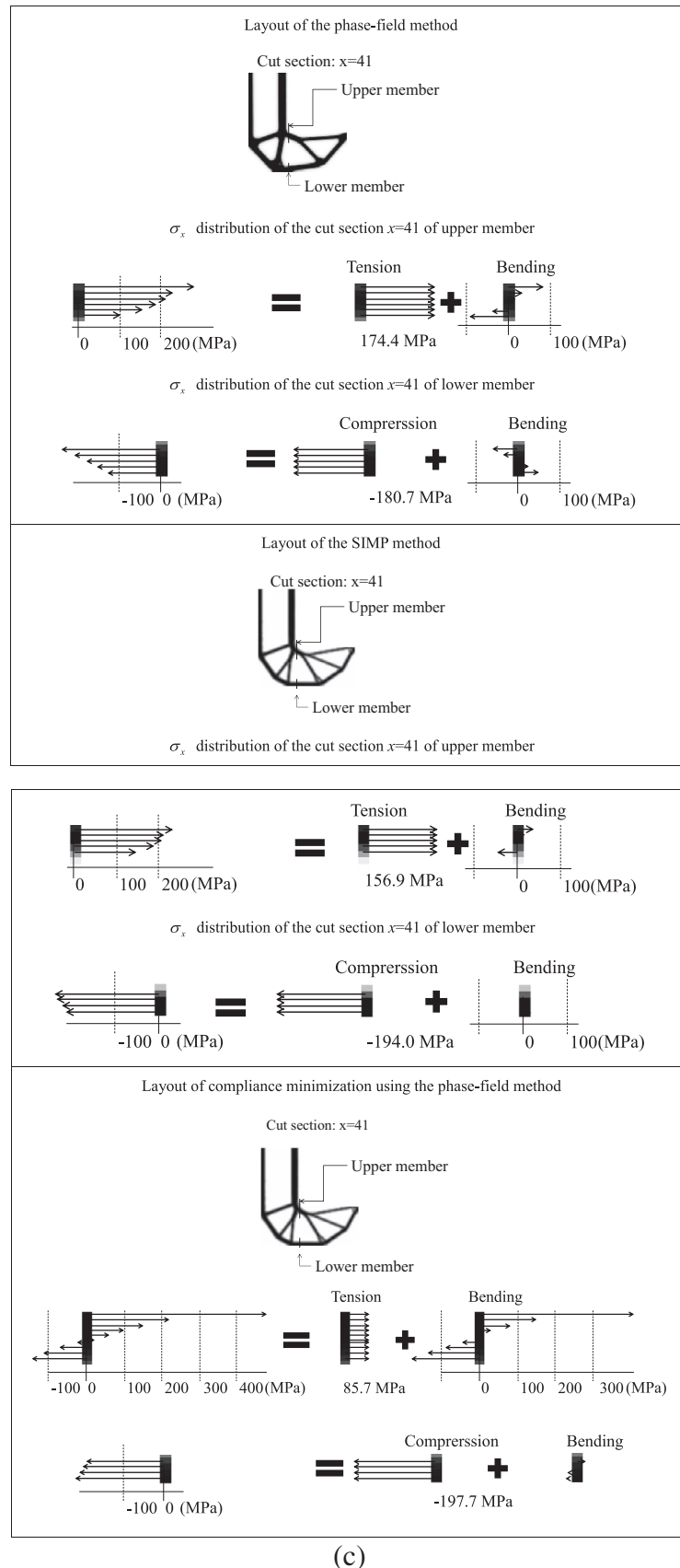


Fig. 8 (continued)

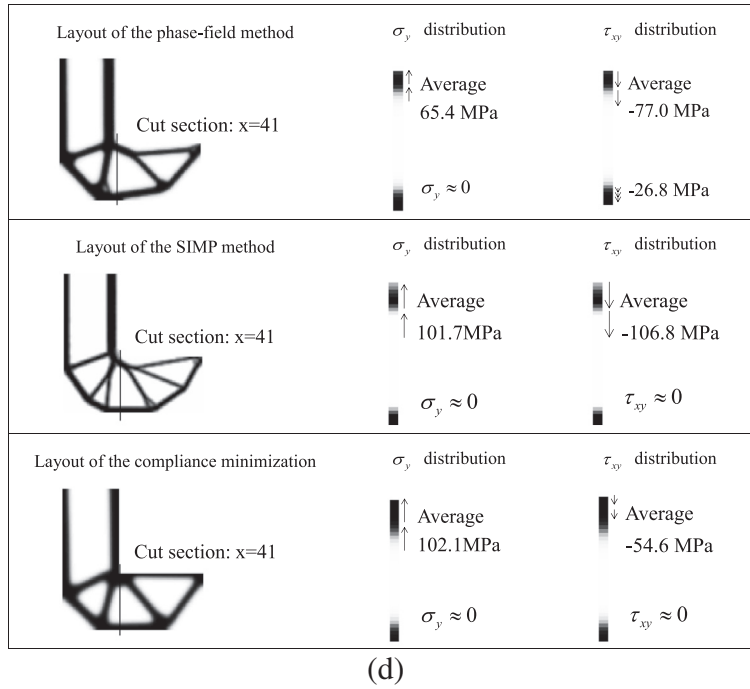


Fig. 8 (continued)

To calculate structural responses, \mathbf{U} , of structures whose topologies are expressed by an explicit phase-field curve, the constitutive matrices are manipulated as follows [22,23].

$$\mathbf{C}_e = \begin{cases} \mathbf{C}_0 & \text{if } \phi_e = 1 \\ k(\phi_e)\mathbf{C}_0 & \text{if } 0 < \phi_e < 1 \\ k_{\min}\mathbf{C}_0 & \text{if } \phi_e = 0 \end{cases} \quad (7)$$

$$k(\phi_e) = k_{\min} + (1 - k_{\min})\phi_e^p \quad (8)$$

where \mathbf{C}_0 and ϕ_e in (7) represent the constitutive matrix of the solid material and the phase-field function value assigned at the e th element, respectively. The scaling factor multiplying the constitutive matrix, which depends on the value of the phase-field curve, is denoted by $k(\phi_e)$. The minimum scaling factor to prevent a singular stiffness matrix and the penalty term are denoted by k_{\min} and p , respectively in (8) [22,23].

For the structural displacement of a topology modeled by the above phase-field, the following static equilibrium equation is solved:

$$\mathbf{KU} = \mathbf{F} \quad (9)$$

where the external force, structural displacement vector, and global stiffness matrix are denoted by \mathbf{F} , \mathbf{U} , and \mathbf{K} , respectively. The above global stiffness matrix is calculated and assembled with the modified constitutive matrices as follows:

$$\mathbf{K} = \sum_{e=1}^{NE} \mathbf{k}_e \quad \text{and} \quad \mathbf{k}_e = \int_{v_e} \mathbf{B}^T \mathbf{C}_e \mathbf{B} dv \quad (v_e : \text{the } e\text{th element domain}) \quad (10)$$

where the stiffness, constitutive, and strain–displacement matrices of the e th element are denoted by \mathbf{k}_e , \mathbf{C}_e , and \mathbf{B} , respectively.

According to previous work on phase-field based topology optimization, the phase-field function commonly evolves via the Allen–Cahn equation (6) to minimize an objective function and satisfy several constraints. The velocities of the phase-field

function are determined by the differences between the heights of the local minima of the double well potential and the curvatures of the interface regions. To move the boundary curves in the direction of minimizing an objective function while satisfying the constraints of the topology optimization, the double well potential is defined as follows:

$$f(0) = 0, \quad f(1) = hf'(\phi_{t_1}), \quad f'(0) = f'(1) = 0 \quad (h > 0) \quad (11)$$

where the gradient of the transformed objective function with respect to the phase-field function is denoted by $J'(\phi)$. (For the gradient calculations for the linear compliance optimization problem, see Appendix A.) It is important to note here that in the original Allen–Cahn equation, only one gradient of the objective function is considered. Therefore, an optimization problem with one objective and several constraints should be transformed into one representative objective function.

3. Implementation of STOM using the framework of the phase-field method

This section reviews the basic concepts and methods associated with stress-based topology optimization (STOM) for linear structures [6,11]. Some new formulations and approaches for an Augmented Lagrange multiplier (ALM) method using a phase-field method will also be developed here. The topological derivative method for local stress constraints is also derived and implemented to make it feasible to generate new holes during design evolution [22,23].

3.1. Stress-based topology optimization formulation

In general, STOM pursues an optimal layout to minimize the use of material or volume subject to local static failure constraints. Here the von Mises stress constraints are taken as the failure constraints. The conventional STOM with explicit curve descriptions can be stated as follows:

$$\begin{aligned}
& \text{Minimize } V(\phi) \\
& \text{subject to } \sigma_e \leq \sigma^* \quad \text{if the } e\text{th element exist} \\
& \quad \quad \quad (e = 1, 2, \dots, NE) : \text{Local constraint} \\
& \quad \quad \quad \phi = [\phi_1, \dots, \phi_{NE}] \quad (\varepsilon \leq \phi_e \leq 1, \varepsilon : \text{a lower bound})
\end{aligned} \tag{12}$$

where σ_e and σ^* represent the element nominal stress, i.e., the von Mises stress and the stress limit value, respectively. The phase-field curve is denoted by ϕ . Because there are too many constraints for locally defined stresses, we convert the above original STOM formulation with the p -norm stress constraints in the segregated design domains by using the SIMP method as follows [6,11]:

$$\begin{aligned}
& \text{Minimize } V(\phi) = \sum_{e=1}^{NE} \phi_e v_e \\
& \text{subject to } \langle \sigma_{\max} \rangle_1 \leq \sigma^* \\
& \quad \quad \quad \langle \sigma_{\max} \rangle_2 \leq \sigma^* \\
& \quad \quad \quad \vdots \\
& \quad \quad \quad \langle \sigma_{\max} \rangle_{RN} \leq \sigma^*
\end{aligned} \tag{13}$$

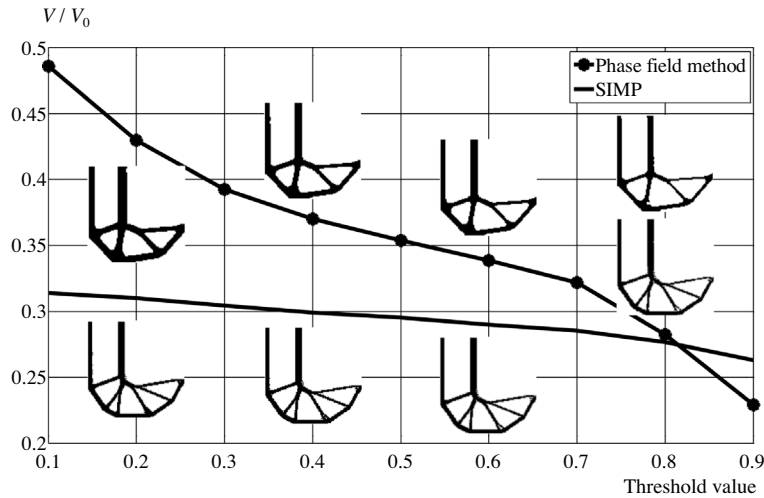
$$\langle \sigma_{\max} \rangle_k \equiv c_k^{iter} \langle \sigma_{PN} \rangle_k \tag{14}$$

$$\langle \sigma_{PN} \rangle_k \equiv \left(\sum_e (\sigma_e)^p \phi_e \right)^{1/p} \quad (e \in \Omega_k) \tag{15}$$

$$c_k^{iter} = \alpha \frac{\sigma_{\max,k}^{iter-1}}{\langle \sigma_{PN} \rangle_k^{iter-1}} + (1 - \alpha) c_k^{iter-1} \quad 0 < \alpha < 1 \tag{16}$$

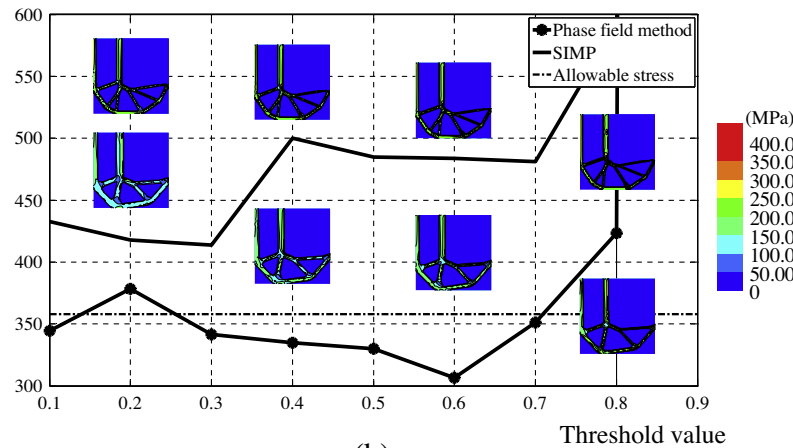
where the phase-field function value assigned to the e th element is denoted by ϕ_e . The approximate maximum stress calculated by the p -norm in the k -th region is $\langle \sigma_{\max} \rangle_k$ and the correction parameter of the p -norm is c_k^{iter} . The nominal maximum stress value at the k th region of the $(iter - 1)$ th iteration is $\sigma_{\max,k}^{iter-1}$. The damping factor α in (16) is adopted for stable convergence of the optimization process and is set to 0.5 for this research. Detailed descriptions of the above formulation can be found in the literature [6,11].

Note that the k th p -norm stress calculation of region Ω_k is defined by considering the magnitude of nominal stress value [11] and is subject to change at each iteration. With the present phase field method, these changes are not recommended because the interfacing regions of the phase field method do not evolve, and the constraints become active. For this reason, we segregate the design domain at the first optimization iteration by sorting finite elements in order of magnitude and employ these regions during the optimization process.



(a)

Maximum stress (MPa)



(b)

Fig. 9. Comparison of post-processing with the SIMP and the phase-field methods for the L-shaped beam: (a) the objective values and layouts according to threshold and (b) the maximum stress values and stress distributions according to threshold value.

3.2. Augmented Lagrange multiplier (ALM) method

The above STOM cannot be solved by the phase-field method directly, as it can only solve an optimization problem with one objective function without constraints with the help of the Allen–Cahn equation. To address the issue of many constraints, we integrate the ALM formulation with the Allen–Cahn equation. As developed and widely known in mathematical optimization theory (see [35] for more detail), the ALM method transforms an optimization problem with many constraints into a problem with only one objective function by using Lagrange multipliers and penalty parameters. For our problem, the objective function (volume) and the constraints (stress) can be integrated into one objective function with the ALM method, which allows us to apply the Allen–Cahn equation. However, since it is not clear how to update the Lagrange multiplier values in the ALM method, we use the mathematical optimization theory behind the ALM method in Eqs. (20) and (21). In other words, the design variables are updated by the Allen–Cahn equation and the Lagrange multipliers are updated through a mathematical formulation.

To clearly explain our proposed hybrid method, consider the following general formulation of the STOM:

$$\begin{aligned} &\text{minimize } f_0(\phi) = V(\phi) \\ &\text{subject to } f_j = \langle \sigma_{\max} \rangle_j - \sigma^* \leq 0 \quad j = 1, \dots, RN \end{aligned} \quad (17)$$

where the objective function and the RN inequality constraints are denoted by f_0 and f_j , ($j = 1, \dots, RN$) respectively. Following [35], the augmented Lagrangian can be formulated as follows:

$$A(\phi, l, r_p) = f_0(\phi) + \sum_{j=1}^{RN} [l_j \Psi_j + r_p \Psi_j^2] \quad (18)$$

$$\begin{aligned} \text{where, } \Psi_j &= \max \left[f_j(\phi), \frac{-l_j}{2r_p} \right] \\ &\cong \frac{f_j(\phi) + \frac{-l_j}{2r_p} + \sqrt{\left(f_j(\phi) + \frac{-l_j}{2r_p} \right)^2 + \varepsilon_s}}{2}, \quad \varepsilon_s \\ &= 2.2204 \times 10^{-16} \end{aligned} \quad (19)$$

The Lagrange multiplier l_j and the penalty parameter r_p are updated at every iteration by the following rule:

$$l_j^{p+1} = \max \left(l_j^p + 2r_p \left\{ \max \left[f_j(\phi), \frac{-l_j^p}{2r_p} \right] \right\}, l_{\max} \right), \quad l_{\max} = 30 \quad (20)$$

$$r_{p+1} = \max(\gamma r_p, r_{\max}), \quad r_{\max} = 10 \quad (21)$$

where the constant scalar γ is adopted to update the penalty parameter and is predefined before the optimization process by an engineer. For this research, γ was set to 2 after some numerical experiments.

3.3. Topological derivatives

Previous research on the application of implicit functions (i.e., level sets or phase fields) discusses the importance of the initial layout on the optimized structure [22,23,26,36,37]. To cope with this issue, the topological derivative method, a heuristic approach, had been developed [23,25,38,39]. This heuristic method introduces new holes inside the structure domain during the evolution based on the topological derivative of the objective function. To do this, the topological derivative estimates the influence of an infinitesimal circular hole on factors relating to the structural response, such as the strain energy. For a simple example, the topological derivative of the volume of a finite element becomes a negative

value of the volume of the element. To efficiently calculate the topological derivative, the adjoint variable method is used. Following the development in [25,39], the adjoint variable of the p -norm stress can be derived as follows:

$$\frac{d\langle \sigma_{PN} \rangle_k}{d\phi_e} = \frac{\partial \langle \sigma_{PN} \rangle_k}{\partial \phi_e} + \frac{\partial \langle \sigma_{PN} \rangle_k}{\partial \sigma_e} \frac{\partial \sigma_e}{\partial \phi_e} + \lambda_k^T \frac{d\mathbf{K}}{d\phi_e} \mathbf{U} \quad (22)$$

$$\mathbf{K}^T \lambda_k = - \sum_{e'=1} \frac{\partial \langle \sigma_{PN} \rangle_k}{\partial \sigma_{e'}} \left(\frac{\partial \sigma_{e'}}{\partial \phi_{e'}} \frac{\partial \sigma_{e'}}{\partial \mathbf{U}} \right)^T \quad (e' \in \Omega_k) \quad (23)$$

The adjoint variable is denoted λ_k . The topological derivative of the p -norm stress in the e th discretized finite element in a design domain can be calculated using the equation below:

$$TD_e^{p\text{-norm}} = -2\sigma(\mathbf{u}_e) : \varepsilon(\lambda_e) = -2\mathbf{u}_e^T \mathbf{k}_e \lambda_{k,e} \quad (24)$$

With the ALM, the final sum of the topological derivative of the volume and the stress constraints becomes the following:

$$TD_e = -v_e + \sum_{k=1}^{RN} l_k (-2\mathbf{u}_e^T \mathbf{k}_e \lambda_{k,e}) \quad (25)$$

3.4. A unified framework for the present topology optimization method

Our topology optimization method, shown in Fig. 5, was implemented using MATLAB. After the initialization process of setting the parameters for the structural analysis, the structural responses, sensitivities of the objective and the constraints, and updates of the phase-field curve by the Allen–Cahn equation are calculated iteratively. A numerical procedure to re-initialize the design domain using the developed topological derivative is performed at every fixed number of iterations.

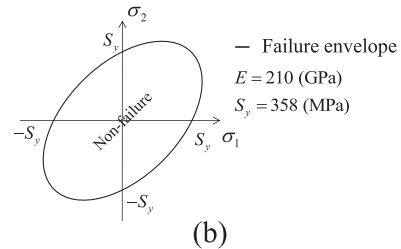
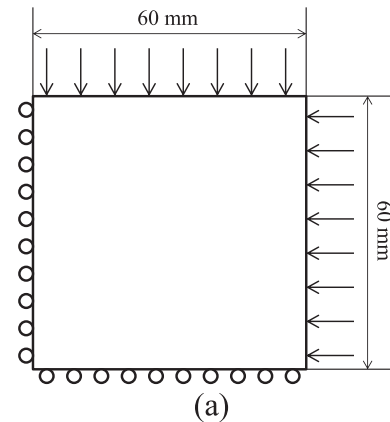


Fig. 10. A plate with a hole. (a) The design domain, the boundary condition, the loading condition (the load is distributed), and (b) the failure envelope of the von Mises stress of the carbon steel of interest.

4. Numerical examples

To show the validity and features of the present phase-field based STOM considering local stress constraints, three benchmark problems, an *L*-shape beam, a plate with a hole and a cantilever beam, are considered. For the sake of illustration of the advantages and disadvantages of the phase-field method compared the classical, density-based topology optimization methods, the optimized layouts and the behaviors of their von Mises stress values are investigated in detail.

4.1. Example 1: an *L*-shaped beam

For the first numerical example, an *L*-shaped beam is considered, as shown in Fig. 6. Because of the stress concentration occurred at the reentrant corner, smooth boundaries should appear, rather than the sharp corner observed in the topological layout given by compliance minimization [6,9,11,40]. The *L*-shaped beam has been studied and optimized by many researches [7–9,40] and Michell truss like structure was investigated in [41,42]. In [2,40], to obtain optimal topologies satisfying the stress constraint, the compliance is considered as an objective or constraint. In [7–9,40], the *L*-shape structure is also optimized by imposing the stress constraints. Despite some differences in the boundary condition, FE mesh, material properties and the optimization method, all the designs satisfy their constraints and the smoothed reentrance corner was emphasized.

Fig. 6 shows an *L*-shape design domain 100×100 mm, which is discretized by 1×1 mm plane stress elements (Q4), the clamp boundary condition at the top and the loading condition. Note that

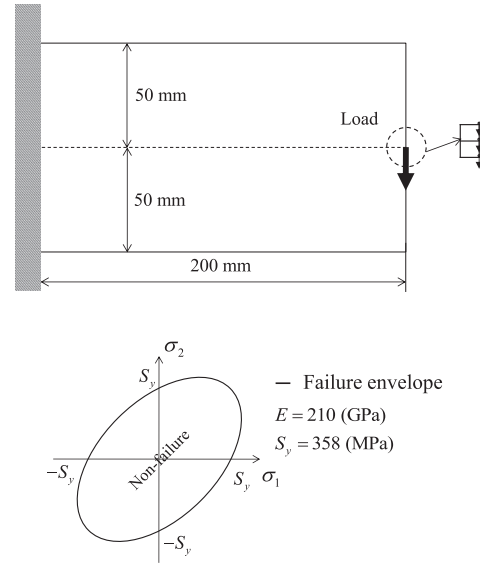


Fig. 12. The design domain, the loading and boundary conditions, and the material properties of the cantilever beam.

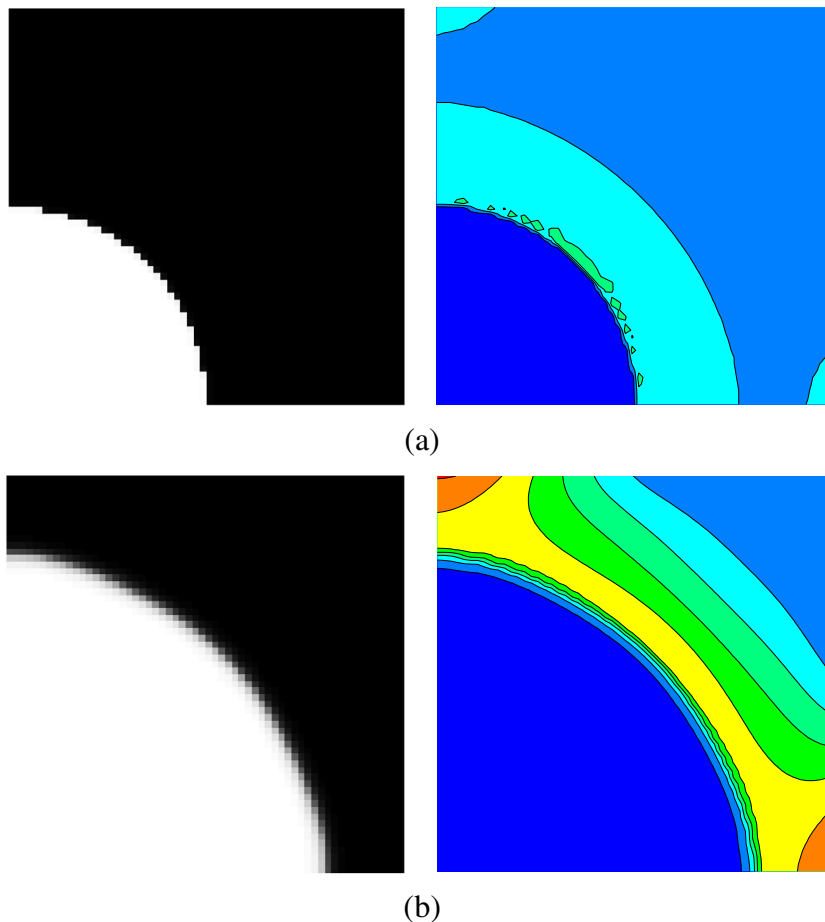


Fig. 11. The initial and the optimized designs. (a) The initial design and the stress distribution of the initial design ($V/V_0 = 0.804$, $\sigma_{\max} = 180.6$ MPa), and (b) the optimized design and the stress distribution of the optimized design ($V/V_0 = 0.519$, $\sigma_{\max} = 356.8$ MPa).

in order to prevent stress concentration at the loading region, the 500 N load is distributed at the top six nodes of the right arm. The Young's modulus, Poisson's ratio and yield stress are set to 210 GP, 0.3 and 358 MPa, respectively, which are those of carbon steel 1144 [43]. The von Mises stresses bounded by the elliptic failure envelope (Fig. 6(b)) are calculated at the centers of all finite elements. The value of p for p -norm stress calculation and the number of regions for p -norm calculation are set to 6 and 4, respectively.

For the sake of illustration of the difficulty and the local optima issue of the present phase-field method, the distribution of the nominal von Mises stress value for the initial layout with five randomly chosen holes is shown in Fig. 7(a). Note that as expected, stress concentrations higher than 358 MPa occur at the reentrant corner, i.e., $\sigma_{\max} = 380.0$ MPa. The present phase-field method minimizing the volume subject to the stress constraints gives the layout of Fig. 7(b), with 36.0% for the mass and 357.9 MPa for the maximum von Mises stress, i.e., the in-active constraints. For comparison, the results of SIMP approach minimizing the volume subject to the constraints and the phase-field approach minimizing compliance subject to a 36.0% mass constraint are also presented in Fig. 7(c and d), respectively. Note that the value of volume frac-

tion is set to the objective value (volume) of the result from the stress-based topology optimization using the phase-field method. This comparison is added to represent that the design minimizing compliance subject to the same volume fraction may result in a structure weak in failure. As expected, the maximum stress value of the stress-based design of Fig. 7(c) is $\sigma_{\max} = 357.7$ MPa and the maximum stress value of the compliance minimization design of Fig. 7(d) is $\sigma_{\max} = 658.9$ MPa. Note that the designs of Fig. 7(b and c) satisfy the local stress constraints (all in-active), and their maximum stress values are under the prescribed maximum stress value. However, the present phase-field based STOM uses more mass, 36% rather than the 29.3% of the density based STOM. From a layout point of view, they are similar but with some differences. To investigate in detail, the stress distributions across some sections of the designs are compared in Fig. 8. First, the reentrance corner of Fig. 7(b) (the present phase-field method) is not smooth, as in Fig. 7(c) (the SIMP method). Nevertheless, the maximum von Mises stress decreases from 380 MPa to 357.9 MPa. The cross sectional area of the vertical beam near the reentrance corner becomes large; see Fig. 8(a). From an objective point of view, the SIMP method is superior to the phase-field method. Second, in

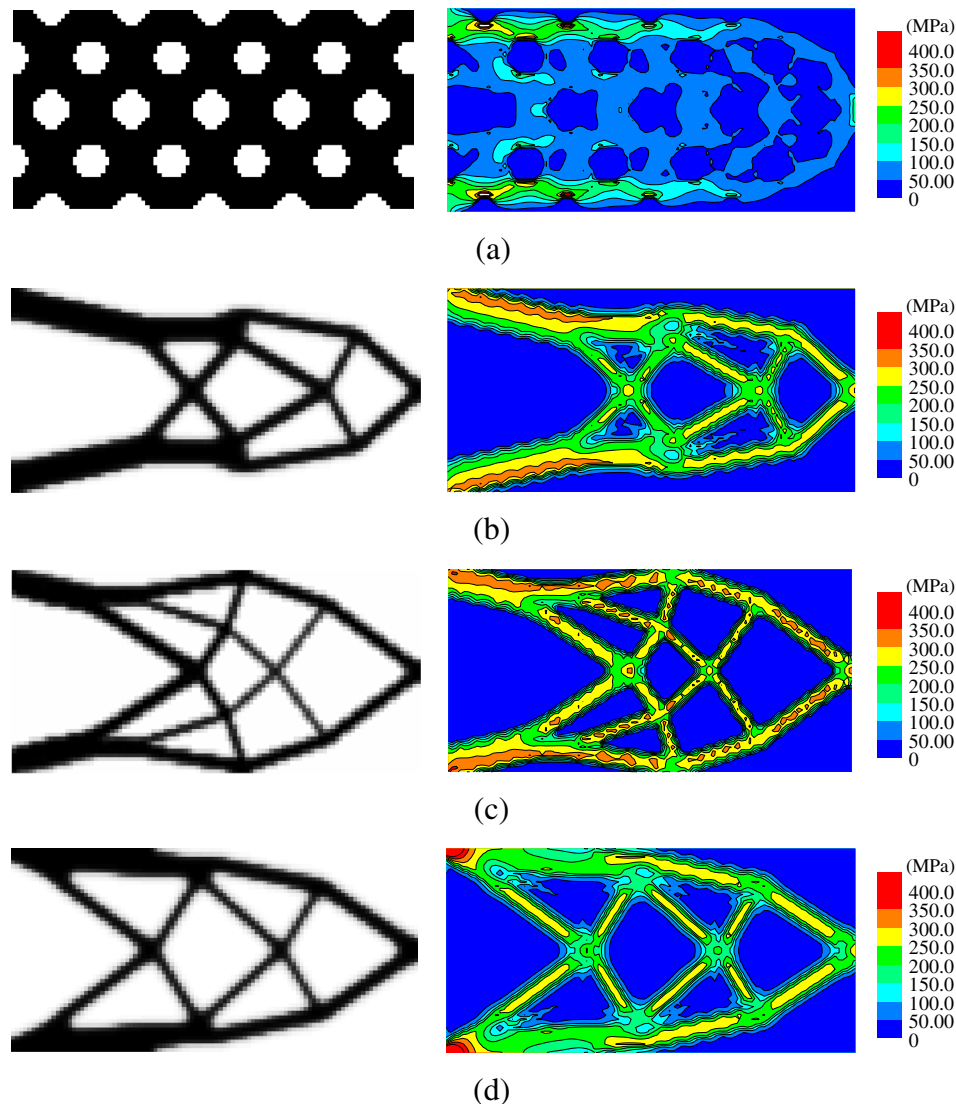


Fig. 13. The initial and the optimized layouts of the cantilever beam: (a) The initial layout and its stress distribution ($\sigma_{\max} = 433.6$ MPa), (b) the optimized layout and its stress distribution obtained by the present stress-based topology optimization method ($V/V_0 = 0.305$, $\sigma_{\max} = 355.1$ MPa), (c) the optimized layout and its stress distribution obtained using the SIMP method ($V/V_0 = 0.278$, $\sigma_{\max} = 358.0$ MPa), and (d) the optimized layout and its stress distribution obtained by solving the compliance minimization problem ($V/V_0 = 0.305$, $\sigma_{\max} = 758.1$ MPa).

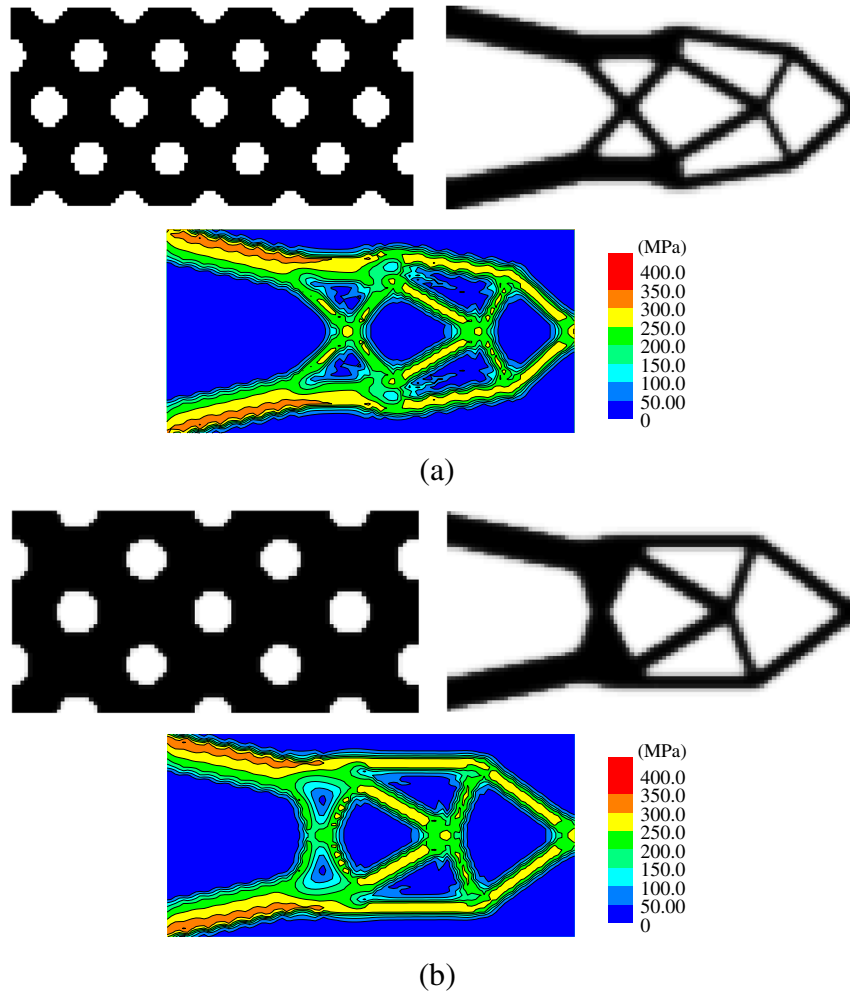


Fig. 14. The effect of the initial layout in the cantilever beam problem: (a) the optimized layout with 27 holes ($V/V_0 = 0.305$, $\sigma_{\max} = 355.1$ MPa) and (b) the optimized layout with 17 holes ($V/V_0 = 0.324$, $\sigma_{\max} = 355.9$ MPa).

Fig. 8(b), in the optimized layout of the present phase-field method, the upper and the down arm members move towards the inside of the design domain. The positions of the four inner reinforcement bars near the reentrance corner in Fig. 8(b) are re-arranged so as to minimize the stress concentration at the reentrance corner. All internal members of the compliance minimization problem are almost normal to the direction of the applied force, and the bending moment due to the external force is mainly resisted at the reentrance corner by the stress distribution of the bending as shown in Fig. 8(c). To the contrary, the internal members of the present stress based design are inclined in the direction of the force, and the stress magnitude due to the bending moment by the external force is smaller than that from the compliance minimization. Finally, based on those observations, it seems that the reduction of the maximum stress is achieved differently by the present phase-field method compared to the density-based STOM.

To explain the above observations in detail, the stress components at the vertical cross sections of the three designs are plotted in Fig. 8. By observing the stress distribution at the cross sections, it is understood that the maximum stress at the corner is decreased in the STOM designs. Due to the intermediate densities of the phase-field method¹ at the center of the graph, some higher von

Mises stress distributions are observed. From the distribution of the stress component in the x direction in Fig. 8(c), it is known that the bending stress at the reentrance corner of the phase field design is smaller than that of the compliance design. In other words, in the phase-field design, a smaller bending moment and extension force are applied, while in the compliance design, a higher bending moment is applied, as explained in Fig. 8(c and d).

4.2. Postprocessing effect of the SIMP method and the phase-field method

After solving the TO by both methods, we performed hard-kill postprocessing, which sets the design variables to 1 or 0 based on a threshold value, as shown in Fig. 9. For the phase-field method, as expected, the design variables in the transition region are post-processed. In Fig. 9, the volumes, the maximum stresses and the layouts after postprocessing are calculated with respect to the threshold value. From a stress point of view, the threshold value for which the postprocessed design becomes feasible is 0.7 for the phase-field case, while there is no such value for the SIMP case. In the SIMP case, the density filter method is used to avoid the checkerboard issue and to cope with highly nonlinear behaviors of the p -norm stress constraints. As a result, many gray elements underestimating stress values appear. Thus, the maximum stress values after postprocessing of the SIMP results are much higher compared to the un-postprocessed design. It is interesting, however, that the results of the phase-field

¹ It has been argued that the intermediate design variables are not a serious issue in the level set or phase field methods. We observe that this is a misleading statement because of the transition region of the level set or phase field methods.

method are relatively stable in terms of maximum stress value after post-processing, even with the intermediate design variables at the transition domain. This may be one of the benefits of optimization methods with explicit curves.

4.3. Example 2: a hole under equal biaxial loading

For a second optimization example, we consider a plate under equal biaxial loading, as in Fig. 10. The design domain is discretized by 1×1 mm plane stress elements (Q4). The value of p for p -norm stress calculation and the number of regions for p -norm calculation are set to 4 and 4, respectively. When applying the SIMP stress-based TO framework with a uniform density distribution that worked for the L -shape structure, a series of failures were experienced and we obtained gray results with some oscillations of the objective function and the stress constraints. However, with the present optimization method and the initial topology of Fig. 10(a), it is possible to obtain the design of Fig. 10(c) by constraining the maximum stress to 358 MPa. Normally the SIMP method provides a better topological design, as the design space exploited by the SIMP method optimizing the material properties of each finite element is larger than that of the phase-field method with explicit curves. However, in this simple plane stress problem, due to the larger design space of the SIMP method, it becomes stuck at local optima. On the other hand, it seems that the phase-field method, with a limited and localized design space, provides a better design, as in Fig. 11. In other words, for this second problem, at least, minimizing volume subject to stress constraints can be solved by the phase-field method.

4.4. Example 3: a cantilever beam

For the third numerical example, we considered a cantilever beam. Fig. 12 shows the 200×100 mm design domain discretized by 1×1 mm plane stress elements, the displacement and loading boundary conditions, and the material properties. The left edge of the design domain is fixed and the distributed load of 1500 N is applied at the center of the right edge. The material properties of carbon steel were again used for this example. The value of p for p -norm stress calculation and the number of regions for p -norm calculation are set to 6 and 4, respectively.

Fig. 13(a) represents the initial layout and its von Mises stress distribution. As the bending stress becomes high at the region near the clamped edge, stress concentration occurs at the edge. Fig. 13(b)–(d) shows the designs obtained by the present phase-field method, the SIMP method minimizing volume subject to the stress constraints, and the phase-field method minimizing compliance with the mass usage of the design of (b), respectively. By investigating the layouts and their von Mises stress values in detail, some conclusions about the designs can be drawn. First of all, in order to relax the stress concentration at the clamped left side, the left side structures of the design are thicker than those in the compliance minimization problem in Fig. 13(b), that is, the stress values become smaller as the cross section areas become large. Second, it seems that the outlines of the present stress design become narrower than those of Fig. 13(d). Compared with the right structural members of the designs of the first L beam example, these narrow structural design changes emerge to minimize the stress values. The effects of the initial layouts of the phase-field method are tested in Fig. 14 and, as expected, different designs are obtained. This example proves again that the size of the design space of the phase-field method is smaller than that of the SIMP method, and the phase-field method using topological derivatives may be classified as a structural optimization method in between topology optimization and shape optimization. In addition, with the phase-field method, local optima issues are always present, but designs with

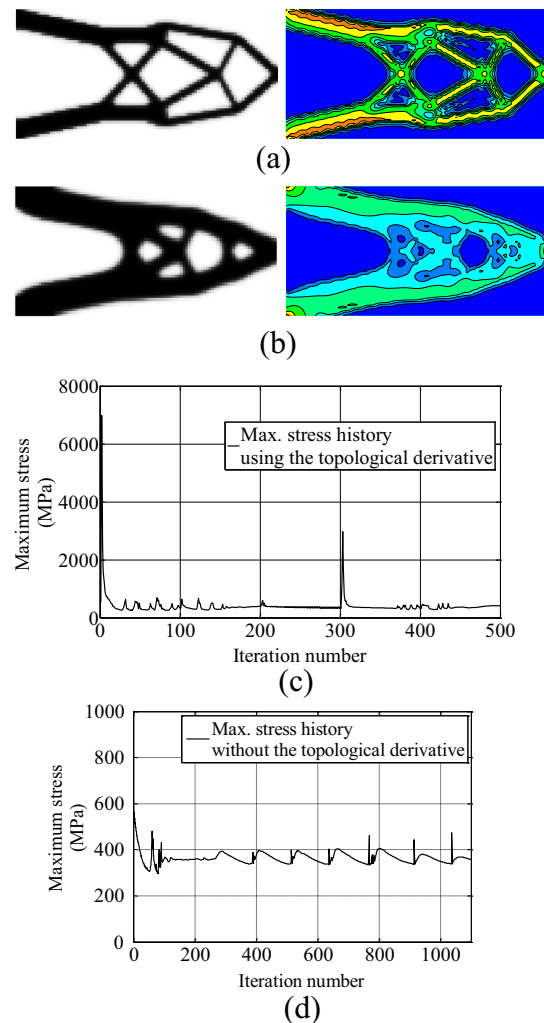


Fig. 15. The effect of the topological derivative for the cantilever beam problem: (a) the optimized layout using the topological derivative ($V/V_0 = 0.305$, $\sigma_{\max} = 355.1$ MPa), (b) the optimized layout without using the topological derivative ($V/V_0 = 0.478$, $\sigma_{\max} = 357.2$ MPa), (c) and (d) the iteration history of the maximum stress with and without the topological derivative, respectively.

solid-void representation with small intermediate design variables are obtainable that is an advantage. In Fig. 15, the effect of the topological derivative is tested. Even without the topological derivative formulation, we can still obtain the design of Fig. 15(b) that satisfies the stress constraints and has smooth convergence. With the topological derivative, however, we experienced some severe discontinuities during the optimization process, and the resulting design of Fig. 15(a) is better than that without the topological derivative in terms of the objective function and stress value.

4.5. Postprocessing effect of the SIMP and the phase-field methods

Similar to the results of the L -shaped beam analysis, the maximum stress values of the phase-field method are smaller than the allowable stress after post processing with threshold values of 0.2 and 0.3. Fig. 16 shows the objective and the maximum stress values as a function of the threshold value.

5. Conclusions

This paper presents a stress-based topology optimization framework which uses phase-field functions to implicitly repre-

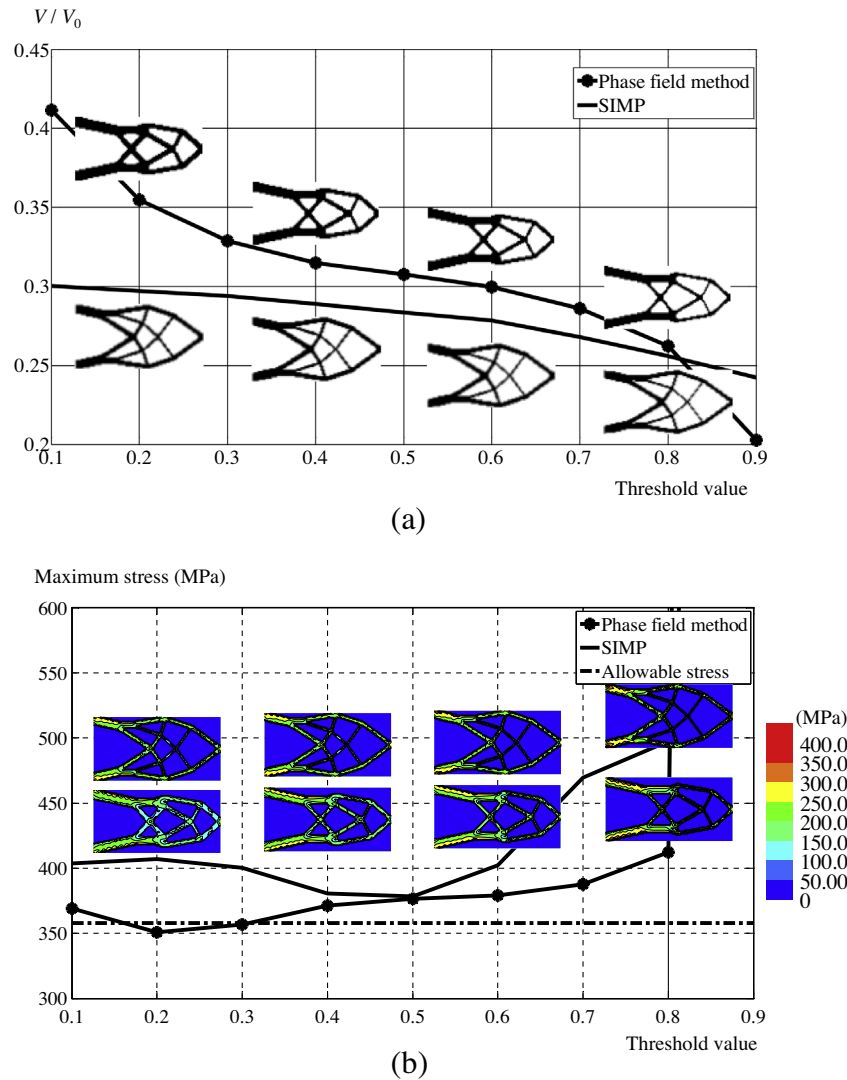


Fig. 16. Comparisons of the SIMP and the phase-field methods for the cantilever beam example in terms of post-processing: (a) the objective values and layouts according to threshold value and (b) the maximum stress values and stress distributions according to threshold value.

sent structural boundaries. Because the present method uses implicit functions to represent structural boundaries, it is possible to perform topology and shape optimization simultaneously. For the implementation of the phase-field method into stress-based topology optimization problems, a new technique combining ALM, phase-field, and topological derivative methods is developed and implemented. With the ALM method, design evolution via the Allen–Cahn equation becomes possible for the structural topology optimization problem to minimize material usage subject to stress constraints. Furthermore, we derive the topological derivative of the global p -norm stress constraint function and apply it to introduce new holes at specified points in the design evolution cycle. The topological derivative allows for an increased design degree of freedom which allows us to obtain better optimized structures. The validity and usefulness of the present method are investigated by solving several structural optimization problems. Numerical results show that the present method gives stable structures satisfying the stress constraints. Comparing the SIMP and the phase-field methods shows that the phase-field method has a smaller design space. Using the optimization examples, we see that the phase-field method is an optimization method between SIMP-based TO methods

and shape optimization methods. Therefore, it is significantly influenced by the initial design, but can still be used as a practical optimization method, allowing for topological changes with solid and void domains with a small number of intermediate domains which are not solid or void. In conclusion, we develop a new phase-field based stress optimization method and investigate its performance and limitations. In the future, it may be possible to extend our method for topology optimization to fatigue constraints (dynamic failures).

Acknowledgement

This work was supported by the National Research Foundation of Korea (NRF) grant funded by the Korea government (MEST) (No. 2012-0005530) and (NRF-2012R1A1A2A10038803).

Appendix A. Topology optimization procedure based on time evolution of the Allen–Chan equation

The topology optimization problem to minimize strain energy subject to volume constraints of a linear elastic system can be stated as follows:

$$\begin{aligned} &\text{Minimize } \mathbf{F}^T \mathbf{U} \\ &\text{subject to } V(\phi)/V_0 \leq V^* \\ &\quad \mathbf{KU} = \mathbf{F} \end{aligned} \quad (26)$$

$$V(\phi) = \sum_{e=1}^{NE} \phi_e v_e \quad (27)$$

$$V_0 = \sum_{e=1}^{NE} v_e \quad (28)$$

where the volume of the e th element and the limit of the volume fraction are denoted by v_e and V^* , respectively.

To create one transformed objective function to minimize strain energy subject to a volume constraint, previous research uses the formulation below:

$$J(\phi) = \mathbf{F}^T \mathbf{U} + \lambda \left(\frac{V}{V_0} - V^* \right) \quad (29)$$

where λ represents a Lagrange multiplier updated at each evolution using the following equation [23].

$$\lambda^{n+1} = 0.5 \left(\lambda^n + \frac{\mathbf{F}^T \mathbf{U}}{V/V_0} \right) + \varepsilon_\lambda \left(\frac{V}{V_0} - V^* \right) \quad (30)$$

One important point should be noted. If the optimized shape is required, the original optimization problem should be transformed into a single objective function to substitute its sensitivities into the Allen–Cahn equation. For stress-based topology optimization, a new transformation method is needed because there are many stress constraint functions to be satisfied.

References

- [1] Bruggi M. On an alternative approach to stress constraints relaxation in topology optimization. *Struct Multidiscip Optim* 2008;36:125–41.
- [2] Bruggi M, Venini P. A mixed FEM approach to stress-constrained topology optimization. *Int J Numer Methods Eng* 2008;73:1693–714.
- [3] Burger M, Stainko R. Phase-field relaxation of topology optimization with local stress constraints. *SIAM J Control Optim* 2006;45:1447–66.
- [4] Duysinx P, Bendsoe MP. Topology optimization of continuum structures with local stress constraints. *Int J Numer Methods Eng* 1998;43:1453–78.
- [5] Jeong SH, Park SH, Choi DH, Yoon GH. Topology optimization considering static failure theories for ductile and brittle materials. *Comput Struct* 2012;110:116–32.
- [6] Le C, Norato J, Bruns T, Ha C, Tortorelli D. Stress-based topology optimization for continua. *Struct Multidiscip Optim* 2010;41:605–20.
- [7] Luo YJ, Kang Z. Topology optimization of continuum structures with Drucker–Prager yield stress constraints. *Comput Struct* 2012;90–91:65–75.
- [8] Paris J, Navarrina F, Colominas I, Casteleiro M. Topology optimization of continuum structures with local and global stress constraints. *Struct Multidiscip Optim* 2009;39:419–37.
- [9] Paris J, Navarrina F, Colominas I, Casteleiro M. Block aggregation of stress constraints in topology optimization of structures. *Adv Eng Software* 2010;41:433–41.
- [10] Svanberg K, Wernke M. Sequential integer programming methods for stress constrained topology optimization. *Struct Multidiscip Optim* 2007;34:277–99.
- [11] Jeong SH, Park SH, Choi DH, Yoon GH. Topology optimization considering static failure theories for ductile and brittle materials. *Comput Struct* 2012;110–111:116–32.
- [12] Yoon GH. Topological design of heat dissipating structure with forced convective heat transfer. *J Mech Sci Technol* 2010;24:1225–33.
- [13] Moon SJ, Yoon GH. A newly developed qp -relaxation method for element connectivity parameterization to achieve stress-based topology optimization for geometrically nonlinear structures. *Comput Meth Appl Mech Eng* 2013;265:226–41.
- [14] Rozvany GIN. Difficulties in truss topology optimization with stress, local buckling and system stability constraints. *Struct Optim* 1996;11:213–7.
- [15] Yang RJ, Chen CJ. Stress-based topology optimization. *Struct Optim* 1996;12:98–105.
- [16] Allaire G, Jouve F, Mailliot H. Topology optimization for minimum stress design with the homogenization method. *Struct Multidiscip Optim* 2004;28:87–98.
- [17] Cheng GD, Guo X. Epsilon-relaxed approach in structural topology optimization. *Struct Optim* 1997;13:258–66.
- [18] Qiu GY, Li XS. A note on the derivation of global stress constraints. *Struct Multidiscip Optim* 2010;40:625–8.
- [19] Verbart A, Dijk N, Tin LD, Langelaar M, Keulen F. Effect of design parameterization and relaxation on model responses in topology optimization with stress constraints. In: *Proceedings of 9th world congress on structural and multidisciplinary optimization*, Shizuoka, Japan, 2011.
- [20] Wang MY, Wang XM, Guo DM. A level set method for structural topology optimization. *Comput Meth Appl Mech Eng* 2003;192:227–46.
- [21] Mei YL, Wang XM. A level set method for structural topology optimization and its applications. *Adv Eng Software* 2004;35:415–41.
- [22] Yamada T, Izui K, Nishiwaki S, Takezawa A. A topology optimization method based on the level set method incorporating a fictitious interface energy. *Comput Meth Appl Mech Eng* 2010;199:2876–91.
- [23] Takezawa A, Nishiwaki S, Kitamura M. Shape and topology optimization based on the phase field method and sensitivity analysis. *J Comput Phys* 2010;229:2697–718.
- [24] Choi JS, Yamada T, Izui K, Nishiwaki S, Yoo J. Topology optimization using a reaction-diffusion equation. *Comput Meth Appl Mech Eng* 2011;200:2407–20.
- [25] Cea J, Garreau S, Guillaume P, Masmoudi M. The shape and topological optimizations connection. *Comput Meth Appl Mech Eng* 2000;188:713–26.
- [26] van Dijk NP, Langelaar M, van Keulen F. Explicit level-set-based topology optimization using an exact Heaviside function and consistent sensitivity analysis. *Int J Numer Methods Eng* 2012;91:67–97.
- [27] Warren JA, Kobayashi R, Lobovsky AE, Carter WC. Extending phase field models of solidification to polycrystalline materials. *Acta Mater* 2003;51:6035–58.
- [28] Singer-Loginova I, Singer HM. The phase field technique for modeling multiphase materials. *Rep Prog Phys* 2008;71.
- [29] Kobayashi R. A brief introduction to phase field method. In: *14th International summer school on crystal growth*, Dalian, 2010.
- [30] Collins JB, Levine H. Diffuse interface model of diffusion-limited crystal-growth. *Phys Rev B* 1985;31:6119–22.
- [31] Kobayashi R. Modeling and numerical simulations of dendritic crystal-growth. *Physica D* 1993;63:410–23.
- [32] Chen LQ. Phase-field models for microstructure evolution. *Ann Rev Mater Res* 2002;32:113–40.
- [33] Biben T. Phase-field models for free-boundary problems. *Eur J Phys* 2005;26:S47–55.
- [34] Allen SM, Cahn JW. Microscopic theory for antiphase boundary motion and its application to antiphase domain coarsening. *Acta Metall* 1979;27:1085–95.
- [35] Vanderplaats GN. *Numerical optimization techniques for engineering design: with applications*. New York: McGraw-Hill; 1984.
- [36] Allaire G, Jouve F, Toader AM. Structural optimization using sensitivity analysis and a level-set method. *J Comput Phys* 2004;194:363–93.
- [37] Amstutz S, Andra H. A new algorithm for topology optimization using a level-set method. *J Comput Phys* 2006;216:573–88.
- [38] Sokolowski J, Zochowski A. On the topological derivative in shape optimization. *SIAM J Control Optim* 1999;37:1251–72.
- [39] Garreau S, Guillaume P, Masmoudi M. The topological asymptotic for PDE systems: the elasticity case. *Siam Journal on Control and Optimization*. 2001;39:1756–78.
- [40] Guo X, Zhang WS, Wang MY, Wei P. Stress-related topology optimization via level set approach. *Comput Meth Appl Mech Eng* 2011;200:3439–52.
- [41] Lewinski T, Rozvany GIN, Sokol T, Bolbotowski K. Exact analytical solutions for some popular benchmark problems in topology optimization III: L-shaped domains revisited. *Struct Multidiscip Optim* 2013;47:937–42.
- [42] Lewinski T, Rozvany GIN. Exact analytical solutions for some popular benchmark problems in topology optimization III: L-shaped domains. *Struct Multidiscip Optim* 2008;35:165–74.
- [43] Budynas RG, Nisbett JK. *Shigley's mechanical engineering design*. 9th ed. New York: McGraw-Hill; 2011.